ELSEVIER

Contents lists available at ScienceDirect

Food Bioscience

journal homepage: www.elsevier.com/locate/fbio





Astaxanthin's anti-angiogenic Effects: Network pharmacology and functional validation in endothelial cells

Anis Zuhaida Mamnun Barizi^a, Muhammad Nazrul Hakim Abdullah^b, Vuanghao Lim^{c,*}, Yoke Keong Yong^{a,**}

- a Department of Human Anatomy, Faculty of Medicine and Health Sciences, Universiti Putra Malaysia, Serdang, 43400, Selangor, Malaysia
- b Department of Biomedical Science, Faculty of Medicine and Health Sciences, Universiti Putra Malaysia, Serdang, 43400, Selangor, Malaysia
- ^c Advanced Medical and Dental Institute, Universiti Sains Malaysia, Bertam, Kepala Batas, 13200, Penang, Malaysia

ARTICLE INFO

Keywords:
Angiogenesis
Migration
Tube formation
Astaxanthin
Network pharmacology

ABSTRACT

Angiogenesis, the formation of new blood vessels from existing ones, is crucial for tumor growth and metastasis. Anti-angiogenic agents are thus a promising therapeutic strategy for cancer. Astaxanthin (ATX), a reddish pigment from the xanthophyll family of carotenoids, may be an effective anti-angiogenic agent due to its notable antioxidant and anti-inflammatory properties. This study aims to investigate the anti-angiogenic effects of ATX on VEGF-induced human umbilical vein endothelial cells (HUVECs). We employed in-silico and in-vitro approaches to evaluate ATX's anti-angiogenic potential. Cytotoxicity assays used concentrations ranging from 50 to $3.125~\mu M$, while other assays utilized concentrations from $25~to~6.25~\mu M$. Network pharmacology identified four hub genes-RXR, CCND1, CDK1, and HDAC1-as key ATX targets against angiogenesis. Molecular docking revealed significant binding affinities of ATX with seven receptors, notably VEGFR2. In vitro, ATX exhibited a dose-dependent cytotoxic effect on HUVECs (IC50 = $75.09 \mu M$), reducing cell viability by 33 % at 50 μM (p<0.05). Additionally, ATX inhibited cell proliferation over 72 h, with significant decreases in VEGF-induced HUVEC viability (p<0.05). The scratch wound healing assay demonstrated ATX's anti-migratory effect, with a 20 % migration rate at 25 μ M over 8 h (p<0.05). Lastly, ATX suppressed tube formation over a 6-h period, significantly reducing average tube length (p<0.05). In conclusion, ATX exhibited significant anti-angiogenic properties through cytotoxicity, inhibition of proliferation, migration, and tube formation in VEGF-induced HUVECs. These findings provide a strong foundation for further research on ATX's potential therapeutic application in angiogenesis-related disorders, including cancer.

1. Introduction

Maintaining physiological homeostasis depends on a delicate balance between agonist and antagonist molecular mediators that regulate critical processes, including angiogenesis—the formation of new blood vessels from preexisting vasculature (Folkman, 1984). While angiogenesis is essential for normal processes such as embryonic growth, wound healing, and the female reproductive cycle, its dysregulation underlies various pathological conditions, including cancer, rheumatoid arthritis, systemic lupus erythematosus, psoriasis, proliferative retinopathy, and atherosclerosis (Dudley & Griffioen, 2023). Particularly in cancer, angiogenesis is considered a hallmark as it facilitates tumor

growth by supplying oxygen, nutrients, and waste removal (Liu et al., 2023). Targeting angiogenesis has thus emerged as a promising therapeutic strategy to inhibit tumor progression by disrupting these vital processes. Among the most prominent signaling pathways in tumor angiogenesis is the VEGF family of growth factors and their receptors (Ahmad & Nawaz, 2022). VEGF inhibitors, such as bevacizumab (Avastin), have been developed to competitively block receptor binding or downregulate VEGF signaling, demonstrating efficacy in inhibiting tumor growth in metastatic colorectal and metastatic breast cancer cancers (Taïeb et al., 2021). However, their use is often accompanied by adverse effects, including hypertension, proteinuria, hemorrhage, gastrointestinal perforation, and poor wound healing (Lopes-Coelho et al., 2021). This highlights the need for novel anti-angiogenic agents

E-mail addresses: vlim@usm.my (V. Lim), yoke_keong@upm.edu.my (Y.K. Yong).

^{*} Corresponding author.

^{**} Corresponding author. Department of Human Anatomy, Faculty of Medicine and Health Sciences, Universiti Putra Malaysia, UPM Serdang, 43400, Selangor, Malaysia.

Abbreviations:		MCC Maximum clique centrality	
		MF	Molecular function
ATX	Astaxanthin	MNC	Maximum neighborhood component
BP	Biological process	MTT	3-(4,5-dimethylthiazol-2-yl)-2,5-diphenyl tetrazolium
CC	Cellular component		bromide
CCND1	Cyclin D1	NCBI	National Center for Biotechnology Information
CDK1	Cyclin-dependent kinase 1	PBS	Phosphate buffer saline
DMSO	Dimethyl sulfoxide	PPI	Protein-protein interaction
FBS	Fetal bovine serum	RXR	Retinoid X receptor
FGFR1	Fibroblast growth factor receptor 1	TIE2	Angiopoietin-1 receptor, Tyrosine-protein kinase recepto
GO	Gene ontology		TEK
HDAC1	Histone deacetylase 1	VEGF	Vascular endothelial growth factor
HUVECs	Human umbilical vein endothelial cells	VEGFR2	Vascular endothelial growth factor receptor 2
IC50	Half-maximal inhibitory concentration	μM	Micromolar
KEGG	Kyoto Encyclopedia of Genes and Genomes	•	

with comparable efficacy but fewer side effects.

Natural products, including carotenoids, offer a promising avenue for discovering novel anti-angiogenic agents. Carotenoids, such as fucoxanthin and siphonaxanthin, have been shown to suppress angiogenesis by inhibiting endothelial cell proliferation and tube formation (Ganesan et al., 2010; Sugawara et al., 2006). Astaxanthin (ATX), a xanthophyll carotenoid with potent antioxidant and anti-inflammatory properties, is a promising candidate for further investigation (Kohandel et al., 2022). ATX (3,3'-dihydroxy-β,β-carotene-4,4'-dione) with a chemical formula of C₄₀H₅₂O₄, is synthesized de novo by various microorganisms, plants, and marine species and is widely consumed by humans via dietary sources like salmon, shrimp, and crustaceans (Aneesh et al., 2022). It is a non-vitamin A, orange to deep-red colour, lipophilic pigment and received the status of generally recognized as safe (GRAS) by the United States Food and Drug Administration (USFDA) (Capelli et al., 2013). The natural ATX which is direct isolated from the natural products are found to be more potent and active in term of the biological activities compared to synthetic one (Capelli et al., 2019). Due to its capability on direct quenching and scavenging free radical species and enhancing antioxidant defence systems in biological system, hence ATX is claimed to be a power antioxidant (Nishida et al., 2023). Extensive studies were conducted to evaluate the antioxidant properties of ATX. Evidence showed that ATX exhibited antioxidant properties by upregulating antioxidant enzyme level, such as GSH-Px, SOD, and CAT, while at the same time down-regulating NADPH oxidase 2 and MDA (Aminullah et al., 2024; Liu et al., 2020). Due to oxidative stress and inflammation fuel each other, anti-inflammatory properties of ATX also been explored. ATX exerted potent anti-inflammatory effect by targeting key pathway, including inhibition of NF-κB activation (Davinelli et al., 2022), reducing pro-inflammatory cytokines (TNF-α, IL-6, IL-1β) (Lee et al., 2024; Wu et al., 2024) and enzymes (COX-2, iNOS) (Masoudi et al., 2021). AST also suppresses MAPK and JAK-STAT signaling (Zhu, Wu, et al., 2022), while enhancing Nrf2 to combat oxidative stress (Liu et al., 2025). Other than abovementioned activities, ATX also reported to possess anti-cancer, neuroprotective, anti-diabetic, and cardioprotective properties (Krestinina et al., 2020; Liu et al., 2020; Penislusshiyan et al., 2020; Sowmya et al., 2017). Beyond these, emerging evidence suggests that ATX also modulates key signaling pathways directly involved in angiogenesis. For instance, ATX has been shown to suppress the expression of vascular endothelial growth factor (VEGF) and its receptors (VEGFR-1 and VEGFR-2), which are central mediators of endothelial proliferation and neovascularization (Izumi-Nagai et al., 2008). This effect is closely linked to the inhibition of the nuclear factor kappa B (NF-κB) pathway, a redox-sensitive transcription factor that regulates multiple proangiogenic and inflammatory genes including IL-6, MCP-1, and ICAM-1 (Speranza et al., 2012). Furthermore, ATX has been

reported to modulate mitogen-activated protein kinase (MAPK) signaling, including ERK1/2 and p38, as well as the phosphoinositide 3-kinase/protein kinase B (PI3K/Akt) axis, both of which are integral to angiogenic signaling (Li et al., 2015; Yang et al., 2019). Despite its broad pharmacological benefits and multiple signaling pathway, its molecular targets and anti-angiogenic properties still remain poorly understood.

This study employs a combination of in-silico (network pharmacology and molecular docking) and in-vitro (cytotoxicity, proliferation, migration, and tube formation assays) approaches to investigate the anti-angiogenic potential of ATX. Network pharmacology was used to predict key ATX target genes involved in angiogenesis, while molecular docking validated their interactions. These computational findings were complemented by in-vitro experiments focusing on endothelial cells, key players in angiogenesis. By addressing the critical stages of angiogenesis, this study seeks to elucidate the potential of ATX as a therapeutic agent for angiogenesis-related disorders, including cancer.

2. Materials and methods

2.1. In silico study

2.1.1. Target prediction of ATX and angiogenesis

ATX target genes were predicted using two distinct databases: the Swiss Target Prediction database (http://www.swisstargetprediction. ch/, accessed on 12 May 2023) and the SuperPred database (https:// prediction.charite.de/index.php, accessed on 12 May 2023). Concurrently, target genes associated with angiogenesis were identified using the keyword "Angiogenesis" across multiple databases to explore potential relationships between ATX and angiogenesis. The databases consulted included DisGeNet (https://www.disgenet.org/, accessed on 12 May 2023), GeneCards (http://www.genecards.org/, accessed on 12 May 2023), and NCBI Gene (https://www.ncbi.nlm.nih.gov/gene/, accessed on 12 May 2023). To ensure specificity, the analysis was restricted to targets identified in *Homo sapiens*. Redundant entries were subsequently removed, and all target names were standardized using the UniProt database. The putative target genes obtained for ATX and angiogenesis were then cross-referenced by intersecting the datasets using InteractiVenn (http://www.interactivenn.net/, accessed on 12 May 2023) to generate a list of common targets.

2.1.2. Compound-target network

The association between ATX and angiogenesis was further analyzed and visualized using Cytoscape software version 3.9.1 (https://cytoscape.org/, accessed on 12 May 2023). The overlapping targets of ATX and angiogenesis, identified through intersection analysis, were organized and categorized before being integrated into Cytoscape. The resulting compound-target network depicted nodes and edges, where

the nodes represented the overlapping target genes of ATX and angiogenesis, and the edges indicated the relationships between them.

2.1.3. Protein-protein interaction (PPI) network analysis

Protein-protein interaction (PPI) network analysis was conducted to further investigate the relationship between ATX and angiogenesis using the STRING database version 11.5 (https://string-db.org/, accessed on 12 May 2023). The analysis was restricted to proteins from *Homo sapiens*, and only interactions with a confidence score of at least 0.900 were included for network visualization. The resulting PPI network was visualized using Cytoscape software, with its relevance assessed through the CytoHubba plugin. Three algorithms—maximum clique centrality (MCC), maximum neighborhood component (MNC), and degree—were employed to identify key genes. The top 10 hub genes, based on confidence scores, were identified by intersecting the results from the three algorithms. These hub genes, considered critical targets for angiogenesis modulation by ATX, were proposed as potential key players for the current investigation.

2.1.4. Gene ontology and pathway enrichment analysis

The Database for Annotation, Visualization, and Integrated Discovery (DAVID) version 2021 (https://david.ncifcrf.gov/home.jsp, accessed on 12 May 2023) was used to perform gene ontology (GO) and Kyoto Encyclopedia of Genes and Genomes (KEGG) pathway enrichment analyses. This analysis provided detailed insights into biological processes, cellular components, molecular functions, and signaling pathways. The top 20 KEGG pathways and the top 10 GO terms were identified and presented. Only statistically significant results with a p-value of less than 0.05 were considered.

2.1.5. Molecular docking

The intersection of the top 10 hub genes identified by the three algorithms revealed four overlapping targets: RXRA, CCND1, CDK1, and HDAC1, which were further evaluated through molecular docking. Additionally, three key tyrosine kinase receptors-VEGFR2, FGFR1, and TIE-2—were included as they are critical regulators in angiogenesis, despite not being listed among the top hub genes. The crystal structures of the four hub genes—RXRA (PDB ID: 7B88), CCND1 (PDB ID: 2W96), CDK1 (PDB ID: 6GU6), and HDAC1 (PDB ID: 4BKX)—and the three tyrosine kinase receptors-VEGFR2 (PDB ID: 3VHE), FGFR1 (PDB ID: 4V05), and TIE-2 (PDB ID: 2WQB)-were retrieved from the RCSB Protein Data Bank (https://www.rcsb.org/, accessed on 19 May 2023). The water from the crystal structure was replaced with hydrogen and designated as receptor. On the other hand, the 3D structure of ATX (Compound CID: 5281224) was obtained from the PubChem database (https://pubchem.ncbi.nlm.nih.gov/, accessed on 19 May 2023). Similarly to the protein receptor, water was deleted and added with hydrogen. Ligand-receptor binding energies were predicted by using AutoDockTools 4.2 (http://autodock.scripps.edu/, accessed on 16 February 2023). The docking parameters were defined in AutoDock by setting the grid center and box size to fully enclose the target protein. Last, the molecular interactions between receptors and ligands were visualized using Biovia Discovery Studio 2021 (https://discover.3ds.co m/discovery-studio-visualizer, accessed on 16 February 2023).

2.2. In vitro study

2.2.1. Chemicals and reagents

Astaxanthin (ATX) (≥97 % HPLC) derived from *Blakeslea trispora* was purchased from Sigma-Aldrich (Germany) and diluted in dimethyl sulfoxide (DMSO) obtained from ATCC (USA). The final DMSO concentration was adjusted to 0.1 %, ensuring non-toxicity to the cells. Vascular endothelial growth factor (VEGF) and suramin were procured from Merck Millipore (Darmstadt, Germany) and Sigma-Aldrich (Germany), respectively. Additionally, phosphate-buffered saline (PBS), 2.5 % trypsin-EDTA solution (10x), 3-(4,5-dimethylthiazol-2-yl)-2,5-

diphenyl tetrazolium bromide (MTT), and Matrigel were purchased from Merck Millipore (Darmstadt, Germany), Santa Cruz Biotechnology (Santa Cruz, CA, USA), Sigma Co. (St. Louis, MO, USA), and BD Biosciences (San Jose, CA, USA), respectively.

2.2.2. Human umbilical veins endothelial cells (HUVECs) culture

Human umbilical vein endothelial cells (HUVECs) were purchased from Merck Millipore (Darmstadt, Germany) and cultured using the EndoGRO-LS Complete Culture Media Kit. The kit included basal medium supplemented with 0.2 % EndoGRO-LS supplement, 5 ng/mL recombinant human epidermal growth factor (rh EGF), 50 $\mu g/mL$ ascorbic acid, 10 nM L-glutamine, 1.0 $\mu g/mL$ hydrocortisone hemisuccinate, 0.75 U/mL heparin sulfate, and 2 % fetal bovine serum (FBS). Low-passage cells (passages 3–6) were used in this experiment. HUVECs were incubated in a humidified incubator at 37 °C with 5 % CO2, and the culture medium was replaced every two days until the cells reached 90 % confluence. Once confluent, the cells were trypsinized using 2.5 % trypsin-EDTA solution (10x), centrifuged at 1200 rpm for 10 min, and subcultured into 25 cm² flasks.

2.2.3. Cytotoxicity assay

Cell cytotoxicity was assessed using the MTT assay, with minor modifications to the previously published method by Devasvaran et al. (2019). Briefly, HUVECs were seeded into 96-well plates at a density of 1 $\times~10^4$ cells/well for overnight and exposed to ATX concentrations ranging from 3.125 to 50 μM on the next day. Following treatment, the cells were incubated at 37 $^{\circ}C$ for another 24 h. Subsequently, 5 μL of MTT solution (2 mg/mL in PBS) was added to each well, and the plates were incubated for an additional 4 h at 37 $^{\circ}C$. The MTT solution was then discarded and replaced with 100 μL of dimethyl sulfoxide (DMSO) to dissolve the purple formazan crystals. The optical density (OD) was measured at a wavelength of 570 nm using an Infinite M200 microplate reader (TECAN, Mannedorf, Switzerland). Cell viability (%) was calculated using the formula:

Cell viability (%) = [Abs (sample)/Abs (control) x 100 %]

The experiment was performed in three independent trials, each conducted in triplicate. Based on the results, three optimal concentrations were selected for subsequent assays. Half-maximal inhibitory concentration (IC $_{50}$) was determined by plotting dose response graph [cell viability (%) versus concentration (μ M)].

2.2.4. Cell proliferation assay

The MTT assay was employed to evaluate cell proliferation, with slight modifications to the methodology described by Kamaruddin et al. (2020). Briefly, HUVECs were seeded into a 96-well plate at a density of 1×10^4 cells/well and co-treated with ATX at concentrations ranging from 6.25 to 25 μM (selected based on the cell cytotoxicity assay) and with the present or absent of 10 ng/mL of vascular endothelial growth factor (VEGF). Group with only cell culture media was served as control. Following treatment, the cells were incubated at 37 °C for 72 h. A baseline group was included and incubated for only 4 h. Subsequently, 5 μL of MTT solution (2 mg/mL in PBS) was added to each well, and the plates were incubated for an additional 4 h at 37 $^{\circ}\text{C}$. The medium was then discarded and replaced with 100 μL of dimethyl sulfoxide (DMSO) to dissolve the purple formazan crystals. The optical density (OD) was measured at a wavelength of 570 nm using an Infinite M200 microplate reader (TECAN, Männedorf, Switzerland). This experimental procedure was performed in three independent tests, each conducted in triplicate.

2.2.5. Migration assay

The evaluation of cell migration was performed using the scratch wound healing assay, based on the procedure described by Ng et al. (2018), with modifications. Briefly, 1.5×10^5 cells/well were seeded into a 24-well plate and cultured for 24 h. Then, the scratch was made in

the cell monolayer using a 200- μ L pipette tip (yellow tip) to mimic a wound. The scratched cells were then washed with PBS to remove any detached cells resulting from the scratching process. Subsequently, HUVECs were co-treated with ATX at concentrations ranging from 6.25 to 25 μ M, along with or without 10 ng/mL of VEGF. Additionally, 20 ng/mL of Suramin, co-treated with 10 ng/mL of VEGF, was used as a positive control. Following treatment, the cells were incubated at 37 °C for 8 h. Images of the gaps were captured at 0 h and 8 h using an inverted microscope equipped with a digital camera (OLYMPUS CKX41, Tokyo, Japan). To ensure consistency, images were taken at the same location for all observations. The gap widths for each experimental group were measured using NIH Image J software (National Institutes of Health, Bethesda, MD, USA; http://imagej.nih.gov/ij/). The results were recorded in length (μ m) and expressed as the migration rate (%) using the formula:

Migration rate (%) = [(The width of initial scratch wound - the width of scratch wound at time 8h)/ The width of initial scratch wound] x 100 %.

This experimental procedure was repeated in three independent tests.

2.2.6. Tube formation assay

The tube formation assay was conducted using Matrigel, following the protocol described by Ng et al. (2018), with modifications. To prevent premature solidification of the Matrigel, the 24-well plate and 1-mL pipette tips were pre-chilled at 4 °C for 30 min before use. Matrigel was loaded in 24-well plate carefully to avoid bubble formation. HUVECs were then seeded onto the solidified Matrigel at a density of 1.5×10^5 cells per well. To ensure successful tube network formation and prevent the formation of cell clusters in the central area, the seeded cells were evenly distributed by gently rotated the plate. Immediately after seeding, 10 ng/mL VEGF and ATX at concentrations ranging from 6.25 to 25 μM were added as a co-treatment, along with the respective control group. The treated cells were incubated at 37 $^{\circ}\text{C}$ for 6 h, after which five random images per well were captured using an inverted microscope equipped with a digital camera (OLYMPUS CKX41, Tokyo, Japan). Tube lengths (µm) in the images were quantified using the angiogenesis plugin in NIH Image J software (http://imagej.nih.gov/ij/). The average tube lengths were calculated from five randomly chosen images per experimental group. Results were expressed as tube lengths (µm). This protocol was repeated in three independent experiments.

2.2.7. Statistical analysis

All numerical data were presented as the mean \pm standard error of mean (Mean \pm SEM) of three independent experiments. Statistical analysis was performed using one-way analysis of variance (ANOVA) followed by Tukey's post hoc test, using GraphPad Prism Version 10 (GraphPad Software, San Diego, CA, USA). Differences between means were considered statistically significant at P < 0.05.

3. Results

3.1. Target and common genes associated with ATX and angiogenesis

Potential target genes of ATX and angiogenesis were identified through multiple databases to establish their correlation. Target genes associated with angiogenesis were retrieved from three databases as of 12 May 2023: GeneCards (7,242 targets), DisGeNET (822 targets), and NCBI Gene (2,141 targets). Concurrently, target genes associated with ATX were obtained from two databases: SuperPred (114 targets) and SwissTargetPrediction (111 targets). Redundant entries were removed and normalized using the UniProt database. A consolidated list was compiled, comprising 7,357 targets associated with angiogenesis and 212 targets associated with ATX. The intersection of these targets, consisting of 171 shared genes, was identified using the online tool

InteractiVenn, as depicted in Fig. 1(A). These 171 overlapping targets were considered potential key target genes and were subjected to further analysis. A detailed list of the associated target genes for ATX and angiogenesis, along with the intersection, is provided in the supplementary materials.

3.2. Compound-target network of ATX and angiogenesis

The relationship between ATX and angiogenesis was further supported by the visualization of the compound-target network constructed using Cytoscape software, as depicted in Fig. 1(B). This visualization demonstrated that ATX and angiogenesis are interconnected through shared common targets.

3.3. PPI network analysis of ATX and angiogenesis

Proteins typically modulate their biological activities through interactions with other proteins and various mechanisms. To elucidate the mechanism of ATX in the treatment of angiogenesis, the STRING database was used to construct a protein-protein interaction (PPI) network based on the 171 intersection targets. After removing isolated nodes and edges, the PPI network comprised 125 nodes and 440 edges, where nodes represent proteins and edges denote their interactions. Using the network analyzer plugin in Cytoscape software, each node was characterized by its degree value: darker colors indicated higher degree values within the network, and lighter colors indicated lower values, as shown in Fig. 2. The analysis revealed that 49 nodes exhibited degree values exceeding the average of 7.04, signifying their strong interconnectivity within the network. Subsequent analysis was performed using the CytoHubba plugin in Cytoscape software. Algorithms such as maximal clique centrality (MCC), maximum neighborhood component (MNC), and degree were applied to identify the top ten hub genes within the constructed PPI network, as depicted in Fig. 3(A). The intersection of the top 10 hub genes identified by these three algorithms resulted in four hub genes—RXR, CCND1, CDK1, and HDAC1 [Fig. 3(B)]. These identified hub genes are pivotal nodes within the network and are hypothesized to play critical roles in the regulatory effects of ATX on angiogenesis.

3.4. GO and KEGG enrichment analysis of targets

To gain a comprehensive understanding of the biological functions of ATX target genes, we conducted Gene Ontology (GO) functional enrichment analysis and KEGG pathway enrichment analysis on the identified targets. Using the DAVID bioinformatics resources, GO analysis revealed a total of 520 biological processes (BPs), 94 cellular components (CCs), and 146 molecular functions (MFs). The top 10 enriched terms in each category (BP, CC, and MF) are presented in Fig. 4(A). The biological processes with the highest enrichment included inflammatory response, protein autophosphorylation, protein phosphorylation, positive regulation of cell proliferation and positive regulation of gene expression. For KEGG pathway enrichment, 153 signaling pathways were identified (p < 0.05). The top 20 pathways, ranked by p-value, are displayed in Fig. 4(B). The most enriched pathways included pathway in cancer, VEGF signaling pathway, chemical carcinogenesis-receptor activation, and viral carcinogenesis. Additionally, other significantly enriched pathways included those involved in neutrophil extracellular trap formation, thyroid hormone signaling, non-small cell lung cancer, and EGFR tyrosine kinase inhibitor resistance. Among these, the "Pathways in cancer" emerged as the top pathway, suggesting that ATX's effects on angiogenesis may be mediated predominantly through cancer-related mechanisms. In summary, this study highlights the potential targets and signaling pathways influenced by ATX, providing valuable insights into its therapeutic potential in angiogenesis. These findings may serve as a foundation for the development of targeted therapies aimed at modulating angiogenesis via ATX.

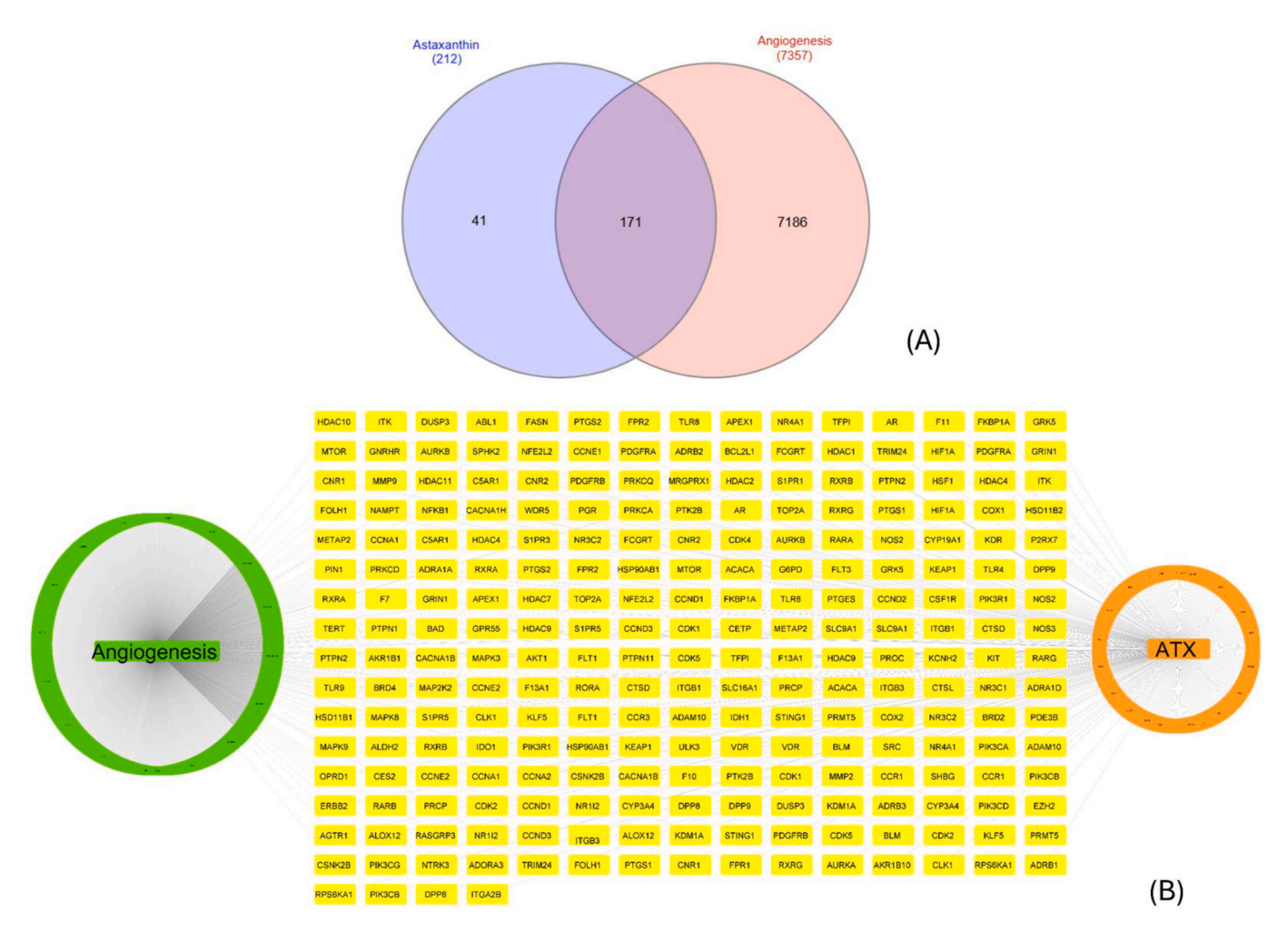


Fig. 1. (A) The intersection of 212 targets of ATX and 7357 targets of angiogenesis resulted in 171 intersected target genes constructed by using InteractiVenn. (B) Compound-target network of 171 intersection targets of ATX and angiogenesis.

3.5. Molecular docking

To further validate the results of the network pharmacology analysis, molecular docking was performed, and the binding energies of each target gene were identified. Despite being key receptors involved in angiogenesis, VEGFR2, FGFR1, and TIE-2 did not emerge in the network pharmacology analysis. Their significance in angiogenesis, however, warrants their inclusion in this study. Phosphorylated VEGFR2 in endothelial cells (ECs) initiates various cellular responses, including significant mitogenic and survival signals, and activates downstream signaling pathways linked to angiogenesis (Shah et al., 2021). FGFR1 is highly expressed in ECs, and its dominant-negative overexpression has been shown to result in pathological angiogenesis (Zhu et al., 2022). Additionally, Tie2 expression and phosphorylation in adult tissues during angiogenesis suggest its critical role in pathological angiogenesis (Duran et al., 2021). Given their well-documented importance, these receptors were included in the molecular docking study to elucidate their interactions with ATX. In this study, the binding energies of the four hub genes identified through network pharmacology-RXR, CCND1, CDK1, and HDAC1-were analyzed alongside the three additional receptors: VEGFR2, FGFR1, and TIE-2. The results revealed that the binding energies for all seven receptors were below -5.0 kcal/mol, indicating significant interactions between ATX and the targets. Among these, the three additional receptors (VEGFR2, FGFR1, and TIE-2) demonstrated the lowest binding energies, suggesting stronger interactions compared to the hub genes identified via network pharmacology. This further justifies their inclusion in the analysis. As displayed

in Table 1, VEGFR2 exhibited the lowest binding energy among all the targets, while RXRA had the highest. Fig. 5 provides 3D and 2D visualizations of the molecular docking interactions for all targets (a–g), showcasing the binding configurations and interactions. These findings highlight the potential role of VEGFR2, FGFR1, and TIE-2 as critical mediators of ATX's effect on angiogenesis.

3.6. Cytotoxicity effect of ATX and its half-maximal inhibitory concentration (IC_{50})

ATX exhibited cytotoxic effects on HUVECs, as demonstrated by a statistically significant reduction in cell viability percentages with increasing ATX concentrations (p < 0.05). At the highest concentration (50 μ M), cell viability was reduced to 67.08 \pm 3.73 %, corresponding to a 33 % decrease in cell population due to ATX's cytotoxic effects. The cell viability percentages for the other concentrations were as follows: 92.88 ± 1.87 % at $3.125~\mu M$, 86.41 ± 4.79 % at $6.25~\mu M$, 79.38 ± 3.56 % at 12.5 μ M, and 77.23 \pm 4.86 % at 25 μ M. Among these, the highest three concentrations (50 μ M, 25 μ M, and 12.5 μ M) showed statistically significant reductions compared to the control group (p < 0.05), as illustrated in Fig. 6 (A). The IC₅₀ value was determined using a simple linear regression analysis, where cell viability (%) was plotted against concentration (µM). The resulting linear equation, Y=-0.5740X+93.10 (R $^{-}$ =0.8385), is depicted in Fig. 6 (B). By solving for X when Y (cell viability) was set to 50 %, the IC50 value was calculated to be 75.09 μ M. This value represents the concentration of ATX required to reduce cell viability by 50 %. Interestingly, the IC₅₀ value

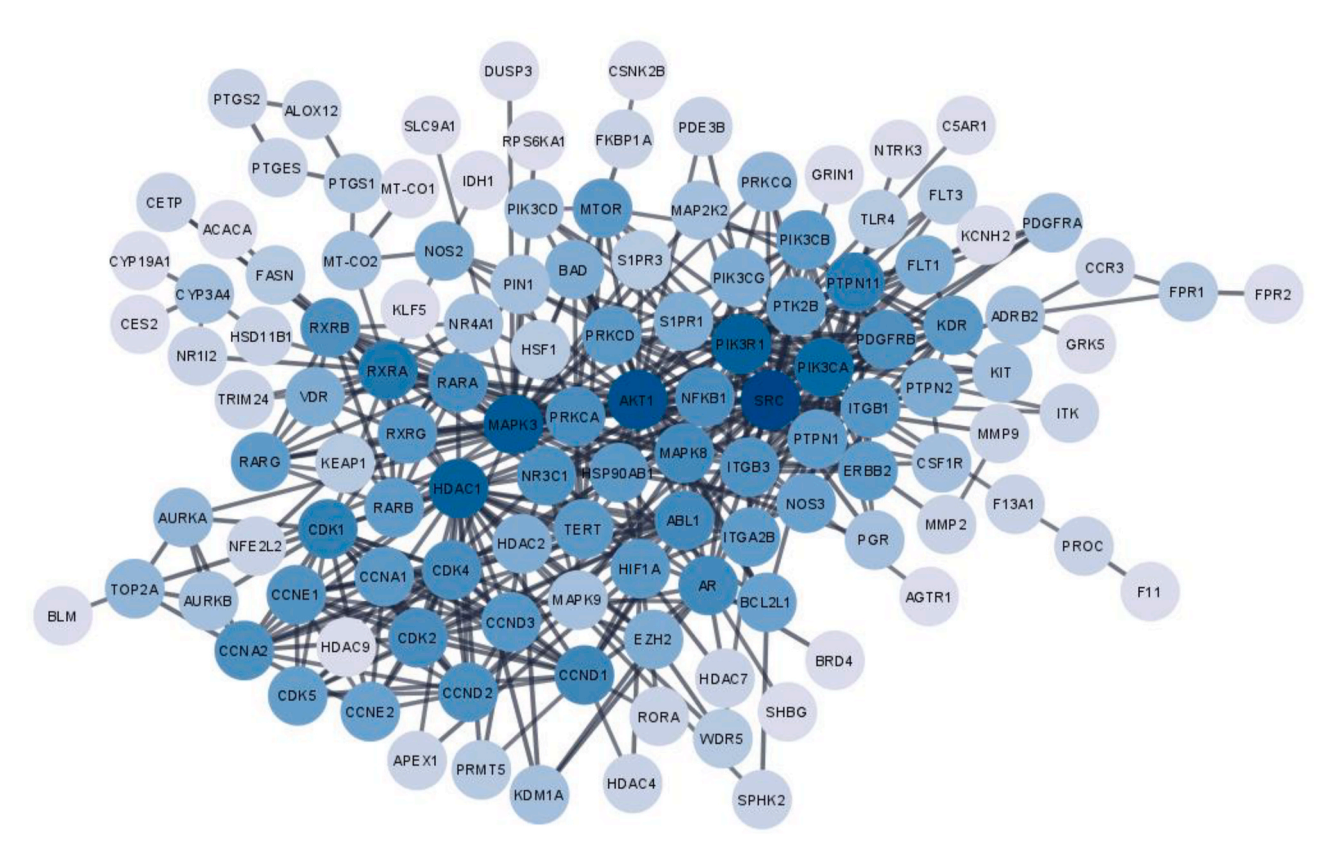


Fig. 2. Protein-protein interaction (PPI) network constructed using STRING database. A greater degree is indicated by a darker shade; hence the shade of circle has been modified in accordance with the degree value.

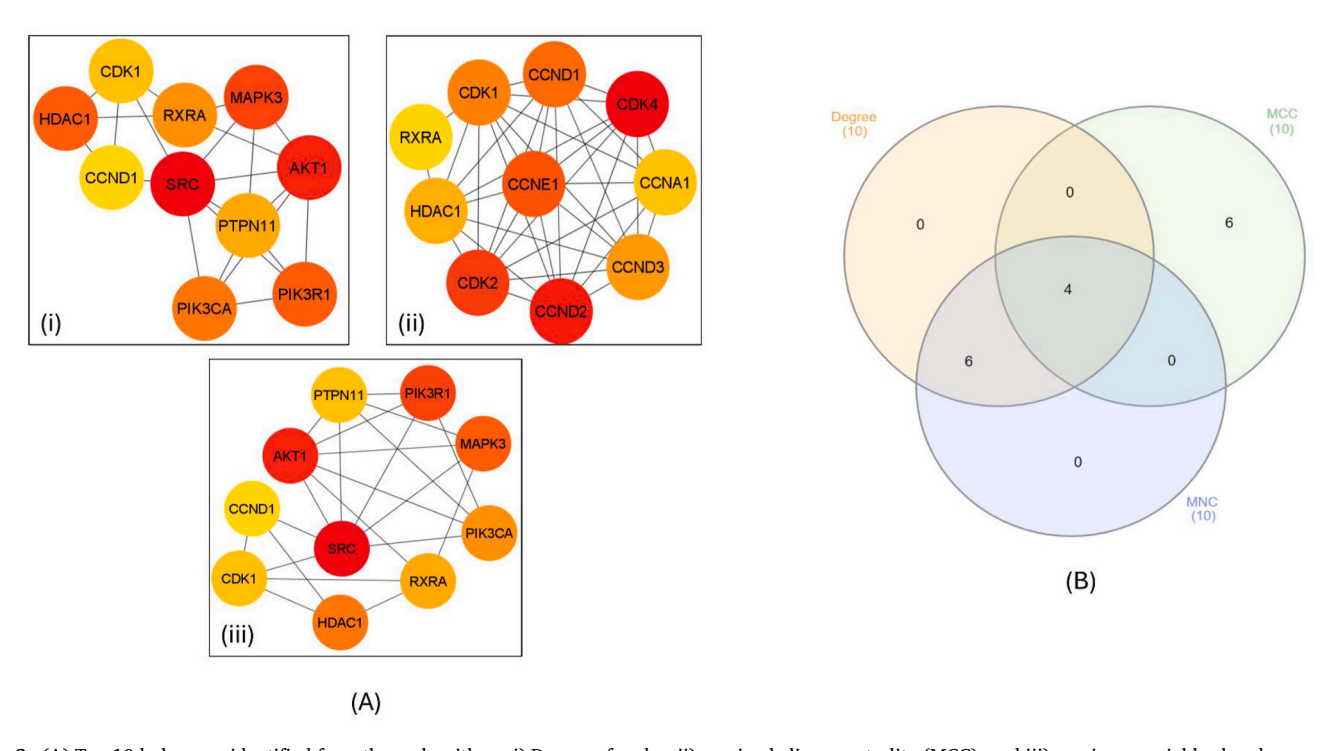
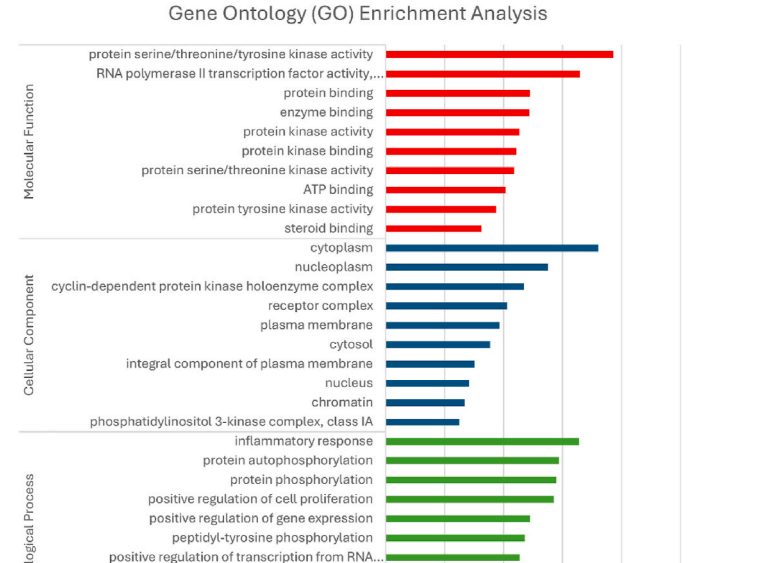


Fig. 3. (A) Top 10 hub genes identified from three algorithms: i) Degree of nodes, ii) maximal clique centrality (MCC), and iii) maximum neighborhood component (MNC). The hub genes that are most significant are those with the highest scores; these genes are indicated in dark red. Conversely, genes with lower scores were thought to be less important and are indicated with a light-yellow colour. (B) The intersection of top 10 hub genes from the three algorithms (degree of nodes, MCC and MNC) visualized by InteractiVenn. The result displayed four target genes— RXR, CCND1, CDK1, and HDAC1.



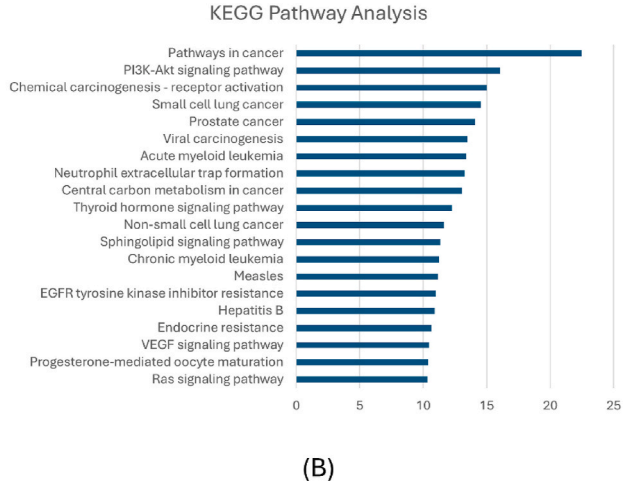


Fig. 4. (A) Gene ontology (GO) enrichment analysis comprising top 10 (log10 (p-value)) of biological process represented by the colour of green (BP), cellular component represented by the colour of blue (CC) and molecular function (MF) represented by the colour of red. (B) The result of top 20 KEGG pathway analysis illustrated by bar chart. Pathway of cancer is the top pathway in this analysis.

Table 1Compound-target molecular docking binding energy.

positive regulation of cell migration

negative regulation of apoptotic process positive regulation of ERK1 and ERK2 cascade

Compound	Targets	PDB ID	Binding Energy (kcal/mol)
ATX	VEGFR2	3VHE	-9.34
	FGFR1	4V05	-9.14
	TIE2	2WQB	-7.61
	CCND1	2W96	-7.55
	CDK1	6GU6	-7.17
	HDAC1	4BKX	-6.60
	RXRA	7B88	-6.42

(A)

(75.09 µM) exceeded the highest tested concentration (50 µM), indicating that the concentrations employed in this study were within a safe range and did not impose excessive toxicity on HUVECs, while still demonstrating cytotoxic effects. Based on these findings, three optimal concentrations—6.25 μ M, 12.5 μ M, and 25 μ M—were selected for subsequent experiments. Pursuant to ISO 10993-5 cytotoxicity classification, a compound is considered non-cytotoxic if cell viability remains above 80 %, while viability between 80 and 60 % is classified as weak cytotoxicity (Serrano et al., 2023). Our findings indicate that ATX at $6.25~\mu M~(86.41~\pm~4.79~\%)$ falls within the non-cytotoxic range, while 12.5 μM (79.38 \pm 3.56 %) and 25 μM (77.23 \pm 4.86 %) exhibit only weak cytotoxicity. At 50 µM, however, ATX significantly reduced cell viability to 67.08 \pm 3.73 %, approaching moderate cytotoxicity. To ensure that our functional assays were conducted within an appropriate and biologically meaningful range, we selected ATX concentrations that maintained at least weak cytotoxicity or higher, avoiding levels that could induce excessive cell death and confound the interpretation of results.

3.7. Anti-proliferation effect of ATX

ATX demonstrated an anti-proliferative effect on HUVECs as assessed through a cell proliferation assay using MTT over 72 h. The results revealed a statistically significant decrease in cell viability percentages

with increasing ATX concentrations (p<0.05). As shown in Fig. 7, the mean cell viability percentages were 141.15 \pm 4.00 %, 122.16 \pm 3.41 %, and 114.50 \pm 5.67 % for ATX concentrations of 6.25 μ M, 12.5 μ M, and 25 μ M, respectively. Although both the VEGF-only group and the ATX-treated group were induced by VEGF, a statistically significant difference (p<0.05) was observed between them, indicating that ATX inhibits HUVEC proliferation even in the presence of VEGF, a known growth factor. Additionally, a 4-h baseline group, comprising media only, was included in the study. The results showed that all treatment groups exposed to ATX for 72 h exhibited significantly higher cell viability values compared to the 4-h baseline group (p<0.05), thereby validating the experimental design.

3.8. Anti-migration effect of ATX

ATX exhibited an anti-migratory effect on HUVECs, as demonstrated through the scratch wound healing assay. This study revealed a statistically significant decrease in migration rates with increasing concentrations of ATX over an 8-h period (p < 0.05). The quantified migration rates for the control group, VEGF-only group, and Suramin group were 31.89 ± 1.00 %, 43.89 ± 2.51 %, and 14.44 ± 0.91 %, respectively. For the ATX-treated groups, the migration rates were 26.00 \pm 1.00 %, 21.44 \pm 1.01 %, and 18.78 \pm 1.04 % for concentrations of 6.25 $\mu M,$ 12.5 $\mu M,$ and 25 μ M, respectively. These data are presented in a bar graph in Fig. 8 (B). The VEGF-only group exhibited the highest migration rate (44 %), surpassing the 32 % migration rate of the control group, which received only medium treatment. VEGF is known to trigger a cascade of protein and enzyme activity that promotes endothelial cell migration across the site of injury represented by the scratched region. Despite VEGF induction, the ATX-treated groups demonstrated statistically significant reductions in migration rates compared to the VEGF-only group (p <0.05). This indicates that ATX exerts an anti-migratory effect on HUVECs, even in the presence of VEGF, a growth factor that typically enhances cell migration. In contrast, the Suramin group, included as a positive control due to its well-known anti-angiogenic properties,

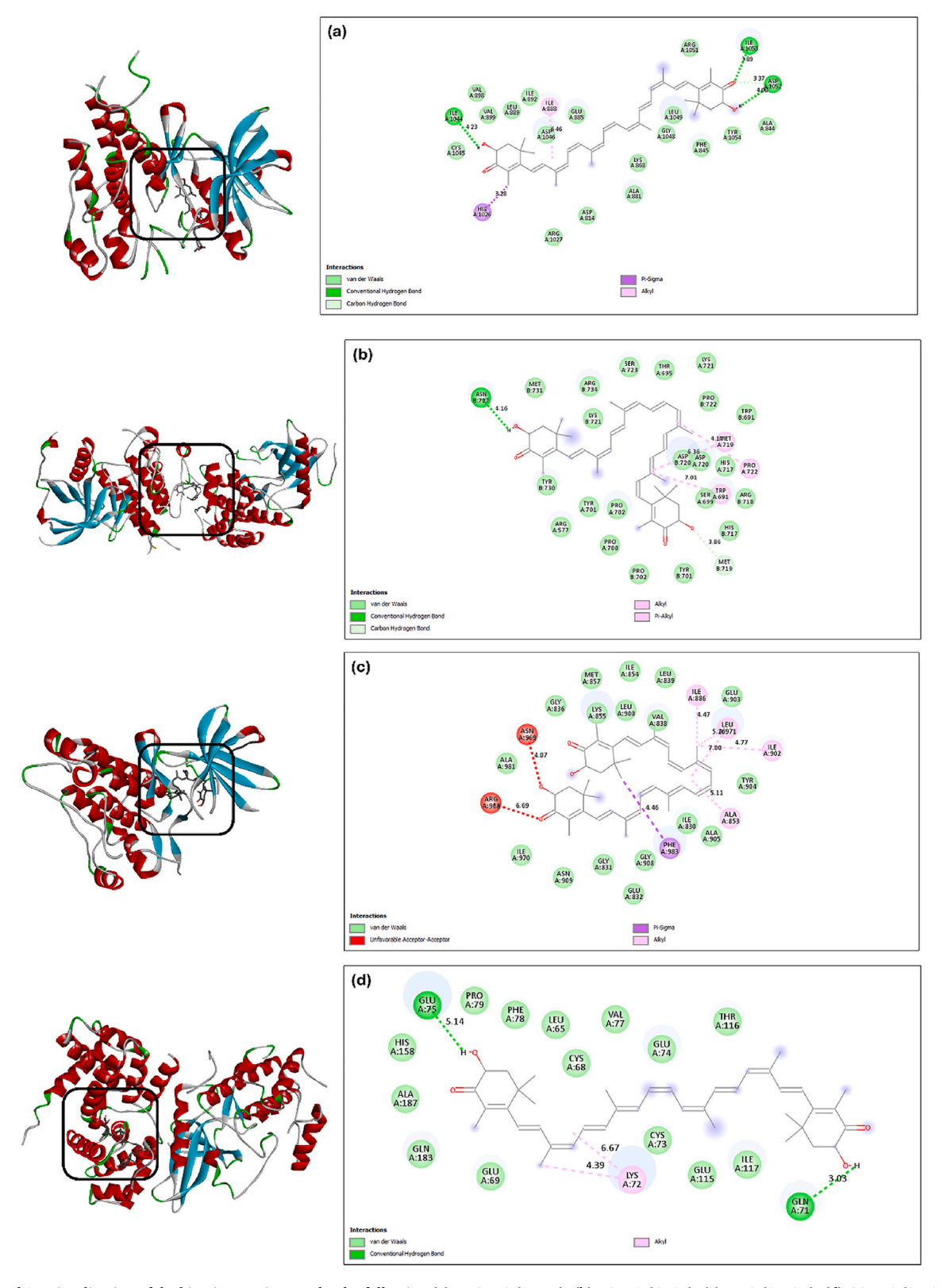


Fig. 5. 3D and 2D visualization of docking interaction results the following (a) VEGFR2 (3VHE), (b) FGFR1 (4V05), (c) TIE2 (2WQB), (d) CCND1 (2W96), (e) CDK1 (6GU6), (f) HDAC1 (4BKX), (g) RXRA (7B88) visualized by Biovia Discovery Studio.

showed a significant reduction in migration rates compared to the control and VEGF-only groups (p < 0.05). Even with VEGF induction, Suramin effectively reduced migration rates to 14 %, validating the experimental design. Representative migration images in Fig. 8 (A)

provide further visual confirmation of these findings.

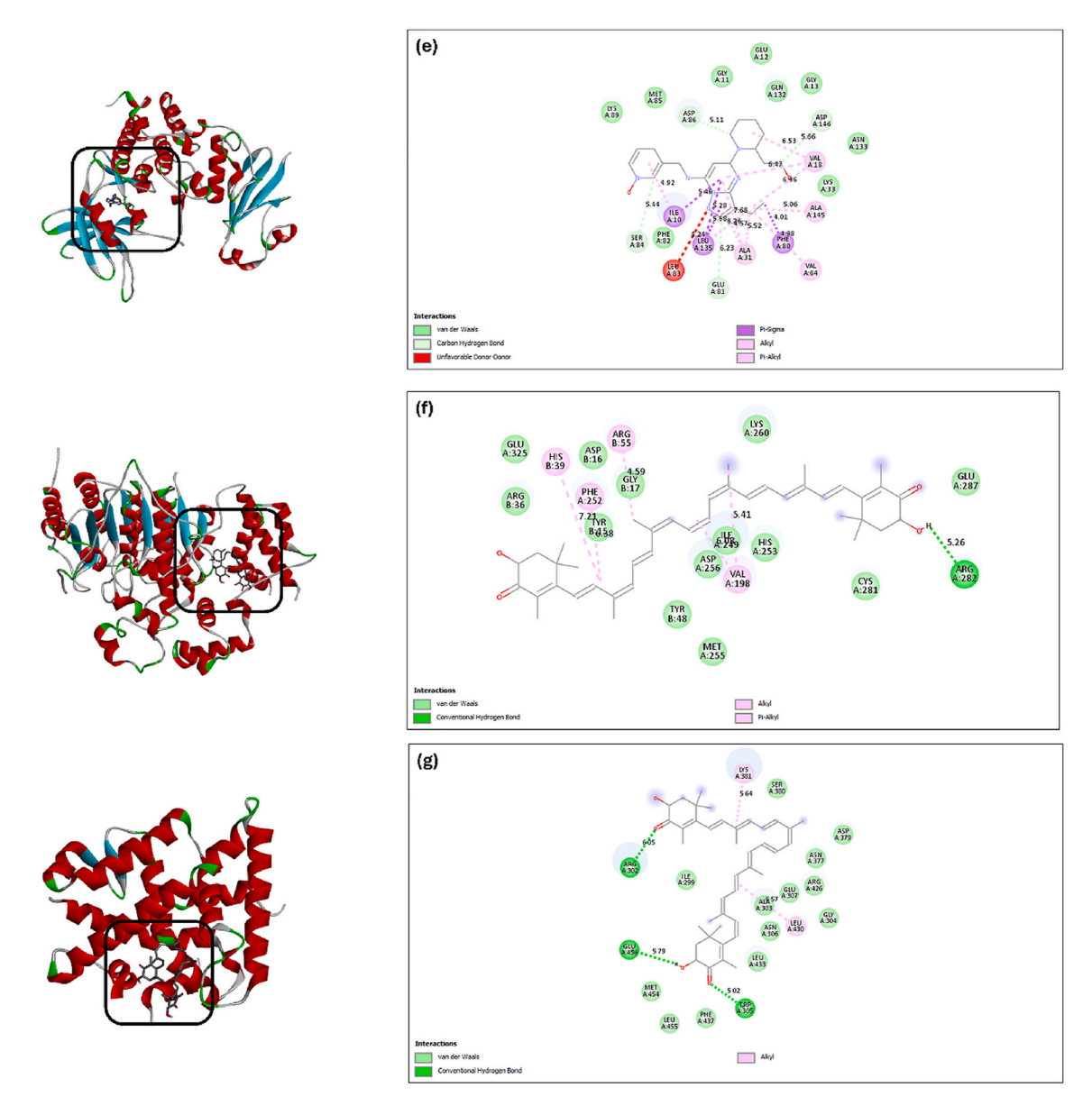


Fig. 5. (continued).

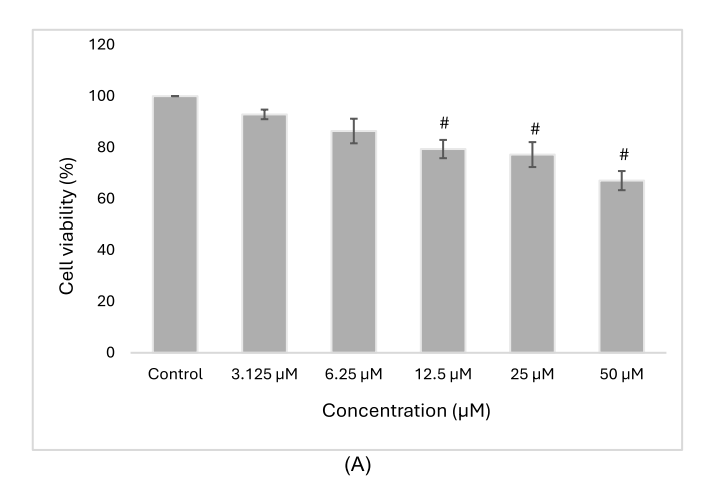
3.9. ATX inhibited VEGF-induced tube formation

ATX inhibited tube formation in HUVECs induced by VEGF, as assessed using a Matrigel-based tube formation assay conducted over 6 h. This study demonstrated a statistically significant reduction in tube length (μ m) with increasing concentrations of ATX (p < 0.05). The measurements revealed mean tube lengths of 4255.89 \pm 234.04 μm for the Suramin group, $9961.44 \pm 529.36 \, \mu m$ for the VEGF-only group, and 7199.67 ± 275.97 µm for the control group. The mean tube lengths for the ATX treatment groups were 5664.11 \pm 364.87 μ m, 5194.22 \pm $235.96~\mu m,$ and $4633.22~\pm~172.42~\mu m$ for ATX concentrations of 6.25 μ M, 12.5 μ M, and 25 μ M, respectively. These data are presented in a bar graph in Fig. 9 (B). The findings indicate that ATX significantly reduced tube formation in a concentration-dependent manner compared to the VEGF-only group (p < 0.05), even in the presence of VEGF. This suggests that ATX effectively inhibits tube formation in HUVECs despite VEGF stimulation. The Suramin group, included as a positive control, also demonstrated a statistically significant reduction in tube length compared to the VEGF-only group (p < 0.05). However, there was no significant difference between the Suramin group and the ATX-treated

groups, suggesting that Suramin, known for its ability to disrupt VEGF signaling, reliably inhibits tube formation. This also implies that ATX may share similar properties with Suramin in its ability to suppress angiogenesis in HUVECs. The morphology and structure of the tube formation further characterize the differences between normal and impaired tube-like structures. Complete tubes and a well-organized network of capillary-like structures indicate normal tube formation, while incomplete tubes, dispersed cells, isolated clumps, and the inability of cells to establish essential connections signify impaired tube formation, resulting in disturbed and fragmented patterns (Xie et al., 2016). Microscopic images of the tube formation results are shown in Fig. 9 (A).

4. Discussion

Angiogenesis is a pivotal process in both physiological and pathological contexts, including cancer progression. As such, targeting angiogenesis has emerged as a promising therapeutic strategy for cancer treatment. Astaxanthin (ATX), a red carotenoid pigment with potent antioxidant properties (Kumar et al., 2022), has drawn significant



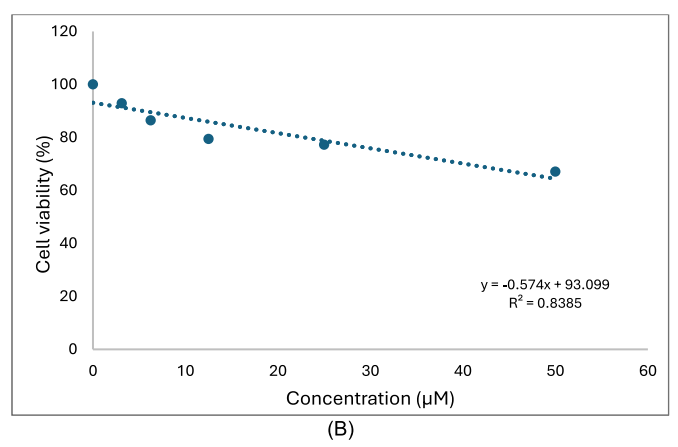


Fig. 6. (A) Cytotoxicity assessment by MTT assay in HUVECs following the exposure of various concentrations of ATX for 24 h. Values are expressed in mean \pm SEM of triplicates and three independent experiments (n=3). Statistical analysis; one-way ANOVA followed by post hoc where statistically significant differences are represented by different letters (P<0.05). (B) Dose response graph by simple linear regression of cytotoxicity assessment utilising MTT assay which plots cell viability (%) versus concentration (μ M) yields the following linear equation: Y = -0.5740 X + 93.10 (R2 = 0.8385). The relevant X value and setting Y (cell viability) to 50 % therefore the calculated IC50 value is 75.09 μ M.

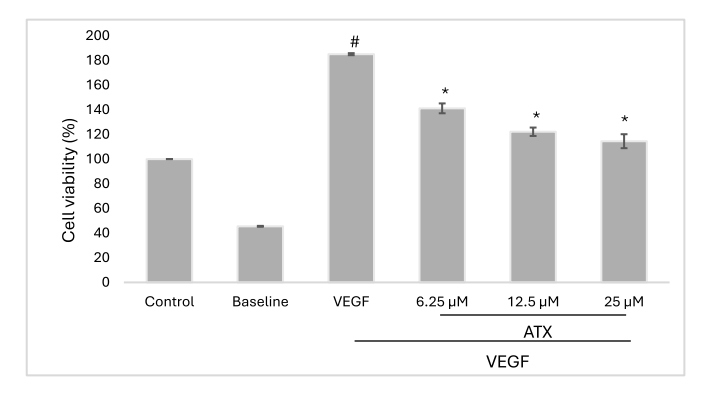


Fig. 7. Anti-proliferative assessment by MTT assay in HUVECs following the exposure of various concentrations of ATX for 24 h 4 h baseline comprising media only was employed as the reference condition. Values are expressed in mean \pm SEM of triplicates and three independent experiments (n=3). Statistical analysis; one-way ANOVA followed by post hoc where statistically significant differences are represented by different letters (p < 0.05).

attention for its potential anti-angiogenic effects. This study explores the

anti-angiogenic properties of ATX through a combination of in silico approaches and in vitro validation.

Network pharmacology, combined with Gene Ontology (GO) and KEGG pathway analyses, offers a comprehensive framework for investigating ATX's biological effects. GO analysis suggests that ATX's antiangiogenic effects are linked to key biological processes, including the inflammatory response, a critical driver of angiogenesis. Inflammation and angiogenesis are intricately connected; inflammatory cells, such as macrophages, secrete signals that stimulate vascular expansion, while angiogenesis can exacerbate inflammation (Jeong et al., 2021). By targeting inflammation, ATX may effectively inhibit angiogenesis. At the molecular level, GO analysis highlights the cytoplasm and protein serine/threonine/tyrosine kinase activity as central components of ATX's mechanism of action. These kinases, including VEGF receptors (VEGFRs), initiate key signaling cascades such as the PI3K/Akt pathway, which regulates endothelial cell migration, proliferation, and survival—key processes in angiogenesis (Peng et al., 2022). KEGG pathway analysis identifies "pathways in cancer" as a top-ranked pathway, underscoring the link between angiogenesis and tumor progression. Tumor cells release pro-angiogenic signals to secure vascular support, preventing necrosis or apoptosis in hypoxic regions (Liu et al., 2023). Additionally, network pharmacology analysis identified four hub genes-RXR, CCND1, CDK1, and HDAC1-that provide a foundation for further exploration of ATX's effects on angiogenesis. Molecular docking revealed strong interactions between ATX and these targets, with VEGFR2 exhibiting the highest binding affinity. The binding energy values (<-0.5 kcal/mol) reflect robust interactions, supporting the hypothesis that ATX may effectively target key proteins involved in angiogenesis. However, while in silico analyses offer valuable predictions, their findings require validation through experimental approaches to establish biological relevance.

The cytotoxicity assay results further support ATX's anti-angiogenic potential. ATX significantly reduced HUVEC viability in a dosedependent manner, highlighting its role in disrupting key processes essential for angiogenesis. Previous studies have reported that ATX exhibits a cytoprotective effect on several normal healthy cells against chemically induced damage (Kikuchi et al., 2020; Kuehu et al., 2024). However, this contradicts our findings, which may be explained by ATX's concentration-dependent effects. At low concentrations, ATX acts as an antioxidant, whereas at higher concentrations, it may exhibit pro-oxidant properties, generating ROS and causing oxidative damage to cellular components, including lipids, proteins, and DNA. Many antioxidants exhibit biphasic behaviour, functioning as antioxidants at low doses while acting as pro-oxidants at higher doses. For instance, selected flavonoids have been shown to promote breast cancer cell proliferation under normal growth conditions while significantly reducing ROS and MDA content at low concentrations. However, at high concentrations, these flavonoids markedly trigger breast cancer cell death through oxidative stress (Xi et al., 2022). Similarly, carotenoid concentration influences its antioxidant or pro-oxidant properties, with high concentrations favouring pro-oxidant behaviour (Valko et al., 2006). The physiological relevance of the ATX concentrations used in this study is supported by pharmacokinetic data from human trials. A study investigating the plasma levels of ATX following oral supplementation of 12 mg per day for one year reported maximum plasma concentrations of 12.1 μM for micellar ATX and 6.47 μM for native ATX in healthy male volunteers (Khayyal et al., 2024). These findings suggest that ATX can reach biologically active concentrations in circulation, particularly with enhanced formulations designed to improve bioavailability. The lower range of concentrations used in this study (6.25–12.5 μ M) aligns with these reported plasma levels, supporting the relevance of our in vitro findings. However, additional studies are needed to determine ATX accumulation in endothelial cells and its long-term effects in vivo. Furthermore, the safety profile of astaxanthin (ATX) has been well-documented in human studies, with multiple clinical trials evaluating its toxicity at varying doses and durations. Studies administering

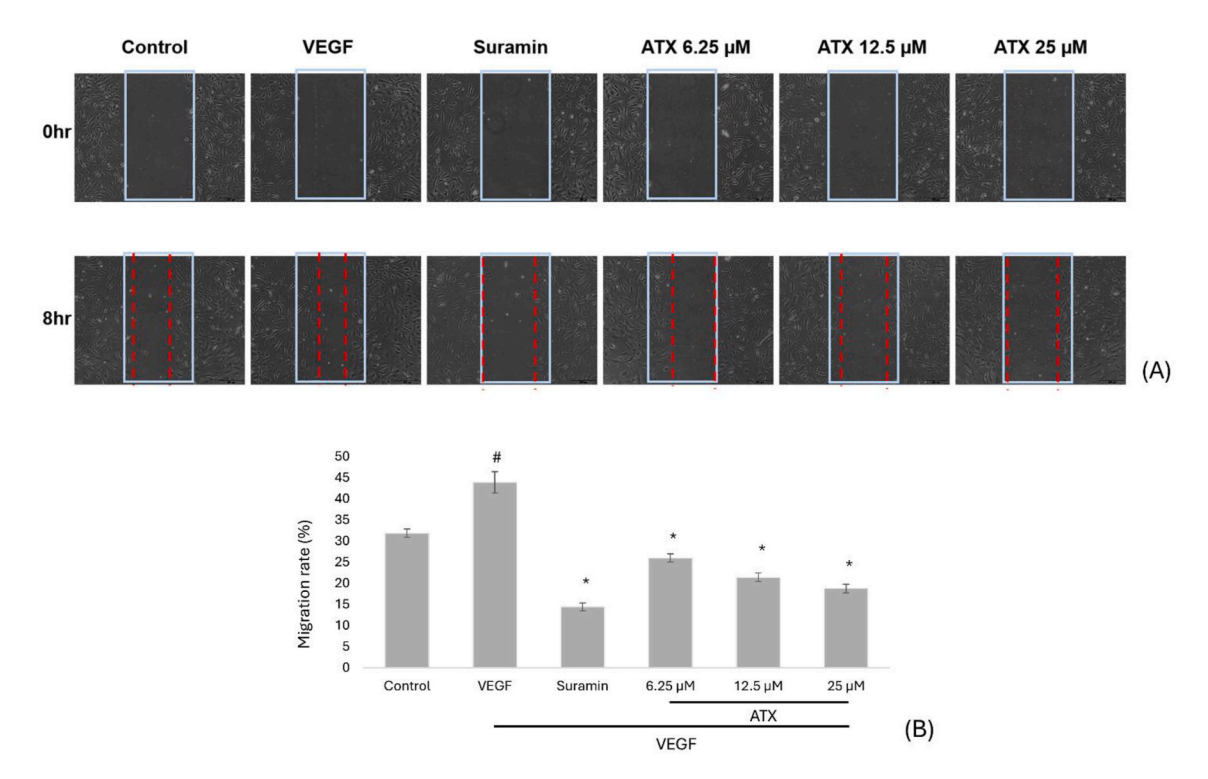


Fig. 8. (A) Anti-migratory assessment by scratch wound healing assay in HUVECs following the exposure of various concentrations of ATX for 8 h. Suramin group comprising suramin and VEGF was employed as the positive control. Values are expressed in mean \pm SD of three independent experiments (n=3). Statistical analysis; one-way ANOVA followed by post hoc where statistically significant differences are represented by # compared to control; * compared to VEGF only (p < 0.05). (B) Wound closure of HUVECs following the treatment of ATX. The white rectangles indicate the initial scratch wound while the red lines indicate the scratch wound at 8 h. VEGF closed before control; suramin closed after both VEGF and control. ATX closed after VEGF but before suramin. At 0 and 8 h, images were taken at a 10x magnification.

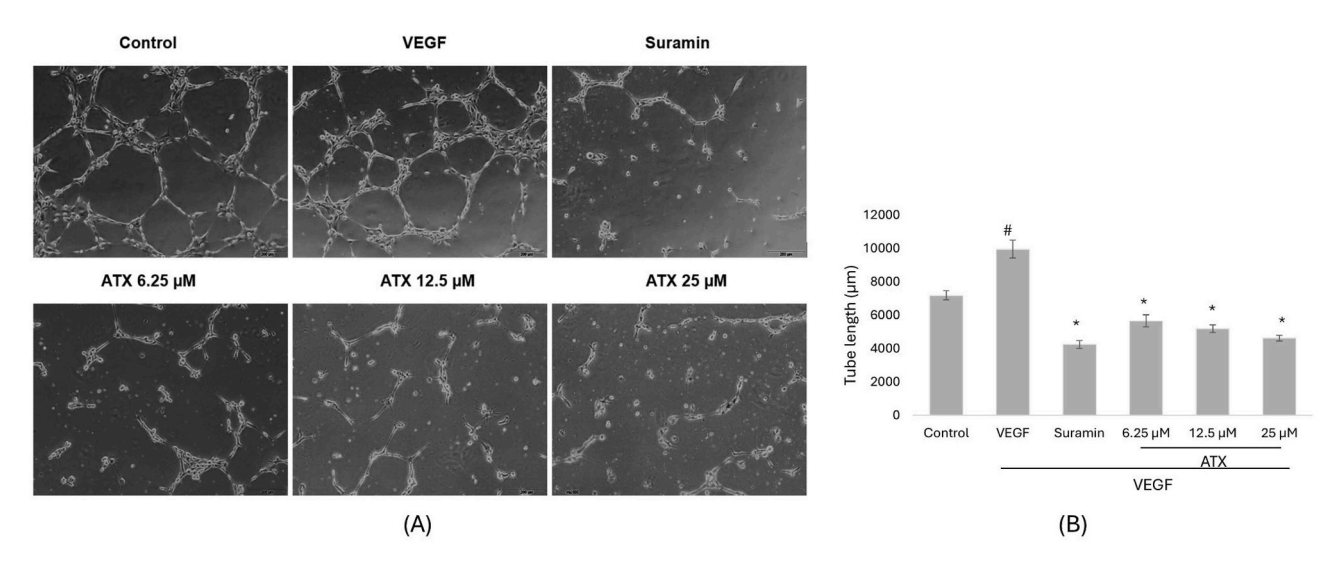


Fig. 9. (A) Microscopic image of tube formation assessment following the exposure of ATX. The control and VEGF-only groups exhibit normal tube formation (complete tube and organised structure), whereas the others exhibit impeded tube formation (incomplete tubes, dispersed cells, and fragmented pattern). At 0 and 6 h, images were taken at a 10x magnification. (B) The inhibition of tube formation by tube formation assay utilising matrigel in HUVECs following the exposure of various concentrations of ATX for 6 h. Values are expressed in mean \pm SEM of three independent experiments (n=3). Statistical analysis; one-way ANOVA followed by post hoc where statistically significant differences are represented by # compared to control; * compared to VEGF only (p < 0.05).

ATX at doses ranging from 6 mg/day up to 45 mg/day for durations between 4 and 12 weeks have consistently reported no significant adverse effects. These studies found no abnormalities in physical examinations, blood tests, urinalysis, or ophthalmic assessments. Furthermore, no incidences of adverse events or side effects were recorded based on medical evaluations (Nishida et al., 2023). These findings indicate that ATX is well-tolerated even at relatively high doses,

supporting its potential for long-term supplementation. However, further investigations are required to determine the safety of chronic high-dose consumption and its potential impact on endothelial function in clinical settings.

Angiogenesis involves a multi-step process, including extracellular matrix remodeling, migration, proliferation, invasion, and tube formation. Among these, endothelial cell proliferation plays a pivotal role in

driving vascular growth. Notably, the proliferation rate has been shown to have a greater impact on the extent and spread of vascular growth than the migration rate (Norton & Popel, 2016). By suppressing endothelial cell proliferation, ATX could impede the vascularization necessary for tumor progression. The anti-proliferative effects of ATX have been demonstrated in various cancer model, also in non-cancerous model, such as hyperoxida-induced retinopathy. A recent study by Kücüködük et al. (2019) investigated the impact of ATX administration via intravitreal and intraperitoneal injections in a C57BL/6J mouse model of hyperoxia-induced retinopathy. The study revealed that ATX significantly reduced neovascular development in both intravitreal and intraperitoneal administration groups compared to controls, highlighting its potential in mitigating pathological angiogenesis. These findings further support ATX's anti-angiogenic potential, reinforcing its role in inhibiting endothelial cell proliferation, a key event in pathological neovascularization.

Endothelial cell migration is a critical component of angiogenesis, governed by three major mechanisms: chemotaxis, haptotaxis, and mechanotaxis (Jerka et al., 2024). Various cytokines, including VEGF, bFGF, and angiopoietins, regulate chemotactic endothelial cell migration during angiogenesis. Under pathological conditions, particularly within the cancer microenvironment, elevated VEGF levels in response to hypoxia promote vascular hyperpermeability, endothelial injury, and migration, ultimately leading to the formation of abnormal blood vessels (Ahmad & Nawaz, 2022). In the present study, VEGF was used to stimulate endothelial cell migration, mimicking tumor angiogenesis. The observed anti-migratory effects of ATX highlight its potential as an anti-angiogenic agent. These findings align with previous studies demonstrating that ATX impedes hypoxia-induced migration in the ECV304 cell line, a derivative of HUVECs (Kowshik et al., 2014). Mechanistically, ATX may exert its effects by downregulating key mediators of hypoxia-driven angiogenesis, including HIF-1a, VEGF, and MMP-2 (Manuelli et al., 2022). Given the central role of hypoxia as a physiological trigger for the angiogenic switch, these results suggest that ATX effectively disrupts hypoxia-driven angiogenic processes. However, further experiments are needed to confirm these findings.

Beyond its anti-migratory effects, ATX suppressed VEGF-induced tube formation in HUVECs, in line with previous studies in ECV304 cells (Kowshik et al., 2014). Tube formation is a critical step in establishing vascular networks, wherein endothelial cells align and connect to form the hollow lumens of new blood vessels. This process is essential for enabling blood flow and delivering oxygen and nutrients to tissues (Trimm & Red-Horse, 2023). The inhibition of tube formation by ATX highlights its potential to disrupt fundamental angiogenic processes. By limiting tube formation, ATX may restrict the blood and nutrient supply to affected tissues, thereby halting the progression of angiogenesis-associated diseases. This effect is particularly significant in pathological conditions like cancer, where excessive angiogenesis supports tumor growth and metastasis.

In the present study, network pharmacology analysis and molecular docking revealed that VEGFR2 exhibited the strongest binding affinity with astaxanthin (ATX), suggesting it as a primary molecular target through which ATX may exert its antiangiogenic effects. These computational findings are supported by existing literature where ATX has been shown to suppress VEGF expression and its receptors (VEGFR-1 and VEGFR-2) (Izumi-Nagai et al., 2008). Inhibition of VEGFR2 likely disrupts key downstream angiogenic signaling cascades, including MAPK and PI3K/AKT pathways. Furthermore, downstream targets such as RXRA, CDK1, and HDAC1—identified as key nodes in the protein protein interaction network—are closely associated with cell cycle progression and epigenetic regulation. Their inhibition by ATX may contribute to the observed suppression of endothelial cell proliferation and neovascularization. RXRA, for instance, modulates transcriptional activity of genes involved in cellular differentiation and metabolism (Zhang et al., 2018), while CDK1 is essential for G2/M phase transition during cell division (Ren et al., 2022). HDAC1, a histone deacetylase,

plays a role in chromatin remodeling and gene repression (English et al., 2025), and it has been linked to angiogenic outcomes (Dunaway & Pollock, 2022). Animal studies have also reinforced the therapeutic promise of ATX in angiogenesis-related conditions. For example, in a hamster model of oral cancer, dietary ATX significantly suppressed carcinoma development by targeting JAK2/STAT3 signaling and reducing the expression of cyclin D1, MMP-2/-9, and VEGF (Kavitha et al., 2013). In diabetic rat models, ATX administration attenuated retinal photoreceptor cell impairments by restoring PI3K/AKT and Nrf2 activity (Lai et al., 2020). These findings align with our in vitro results and support the translational relevance of ATX as a bioactive nutraceutical for angiogenesis-associated disorders. Together, these in silico and in vitro findings provide a comprehensive mechanistic insight into the antiangiogenic effects of ATX and support its therapeutic potential in targeting angiogenesis-related diseases. However, further exploration is warranted to validate its efficacy and uncover additional molecular targets.

5. Conclusion

This study identifies RXR, CCND1, CDK1, and HDAC1 as key hub genes implicated in the anti-angiogenic effects of ATX through network pharmacology analysis. GO enrichment revealed that ATX may act by modulating inflammatory responses (biological process), targeting the cytoplasm (cellular component), and influencing protein serine/threonine/tyrosine kinase activity (molecular function). Pathway analysis highlighted the cancer pathway as a primary target in angiogenesisrelated mechanisms. Molecular docking confirmed ATX's strong binding affinities to VEGFR2, FGFR1, TIE2, and the four hub genes, with the highest affinity for VEGFR2. Experimental findings demonstrated ATX's cytotoxicity (IC50: 75.09 μ M), anti-proliferative, anti-migratory, and tube formation-inhibitory effects on VEGF-induced HUVECs. Collectively, these findings highlight ATX's multi-faceted anti-angiogenic effects, spanning inflammation modulation, cytotoxicity, migration inhibition, and tube formation suppression. While these results provide valuable insights, further validation through in vivo models and advanced techniques, such as transcriptomics or metabolomics, is essential to uncover additional molecular targets and pathways. Investigating ATX's bioavailability, pharmacokinetics, and potential offtarget effects will also be crucial for clinical translation. By integrating computational and experimental approaches, this study establishes ATX as a promising therapeutic candidate for mitigating aberrant angiogenesis, paving the way for future research on its application in combination therapies or as a standalone intervention for angiogenesisdriven diseases.

6. Limitation and future research directions

A major limitation of this study is the lack of in vivo validation, as the anti-angiogenic effects of astaxanthin (ATX) were only assessed in vitro. While our findings demonstrate that ATX inhibits endothelial cell migration, proliferation, and tube formation, its efficacy in a physiological setting remains uncertain. Additionally, although the concentrations used were selected based on cytotoxicity assays, the physiological relevance of these doses in vivo requires further confirmation, particularly in relation to ATX's bioavailability and accumulation in endothelial tissues. Furthermore, while in silico analysis identified key angiogenic targets modulated by ATX, direct experimental validation of these targets at the gene and protein levels was not performed, limiting our mechanistic understanding of ATX's mode of action. To overcome these limitations, future studies should focus on in vivo models of pathological angiogenesis to validate ATX's antiangiogenic potential under physiological conditions. Additionally, pharmacokinetic studies are needed to determine ATX's bioavailability, metabolism, and distribution, particularly in endothelial tissues, to establish whether the concentrations used in vitro are achievable in

vivo. Further mechanistic investigations should also be conducted to confirm ATX's modulation of predicted molecular targets through gene and protein expression analyses. Moreover, research should explore advanced formulation strategies, such as nanocarriers or micellar systems, to enhance ATX's stability, absorption, and targeted delivery, ultimately improving its therapeutic efficacy.

CRediT authorship contribution statement

Anis Zuhaida Mamnun Barizi: Writing – review & editing, Writing – original draft, Project administration, Formal analysis, Data curation, Conceptualization. Muhammad Nazrul Hakim Abdullah: Writing – original draft, Validation, Formal analysis, Conceptualization. Vuanghao Lim: Writing – review & editing, Validation, Supervision, Methodology, Formal analysis, Conceptualization. Yoke Keong Yong: Writing – review & editing, Validation, Supervision, Methodology, Funding acquisition, Formal analysis, Conceptualization.

Ethics approval and consent to participate

Not applicable.

Consent for publication

Not applicable.

Availability of data and materials

The datasets used and/or analyzed during the current study are available from the corresponding author on reasonable request.

Funding

This study was supported by the University Grant, Geran Putra – Inisiatif Putra Siswazah (GP-IPS/2017/9576700) under Universiti Putra Malaysia.

Declaration of competing interest

The authors declare the following financial interests/personal relationships which may be considered as potential competing interests: Not applicable.

Acknowledgements

This study was supported by the University Grant, Geran Putra – Inisiatif Putra Siswazah (GP-IPS/2017/9576700) under Universiti Putra Malaysia. The authors would like to thank all the supporting staff from the Anatomy and Histology Laboratory for their kind assistance during the project.

Appendix A. Supplementary data

Supplementary data to this article can be found online at https://doi.org/10.1016/j.fbio.2025.106972.

Data availability

Data will be made available on request.

References

Ahmad, A., & Nawaz, M. I. (2022). Molecular mechanism of VEGF and its role in pathological angiogenesis. *Journal of Cellular Biochemistry*, 123(12), 1938–1965.
 Aminullah, Y., Naftali, Z., Santosa, D., Prajoko, Y. W., Azam, M., Susanto, H., & Subagyo, H. W. (2024). Boosting antioxidant defense: The effect of astaxantin on superoxidase dismutase and malondialdehyde reduction in patients with head and

- neck cancer receiving cisplatin chemotherapy. Asian Pacific Journal of Cancer Prevention, 25(10), 3741–3748.
- Aneesh, P. A., Ajeeshkumar, K. K., Lekshmi, R. K., Anandan, R., Ravishankar, C. N., & Mathew, S. (2022). Bioactivities of astaxanthin from natural sources, augmenting its biomedical potential: A review. *Trends in Food Science & Technology*, 125, 81–90.
- Capelli, B., Bagchi, D., & Cysewski, G. R. (2013). Synthetic astaxanthin is significantly inferior to algal-based astaxanthin as an antioxidant and may not be suitable as a human nutraceutical supplement. *Nutrafoods*, 12(4), 145–152, 2013 12:4.
- Capelli, B., Talbott, S., & Ding, L. (2019). Astaxanthin sources: Suitability for human health and nutrition. Functional Foods in Health and Disease, 9(6), 430–445.
- Davinelli, S., Saso, L., D'Angeli, F., Calabrese, V., Intrieri, M., & Scapagnini, G. (2022). Astaxanthin as a modulator of Nrf2, NF-kB, and their crosstalk: Molecular mechanisms and possible clinical applications. *Molecules (Basel)*, 27(2), 502.
- Devasvaran, K., Tan, J. J., Ng, C. T., Fong, L. Y., & Yong, Y. K. (2019). Malaysian tualang honey inhibits hydrogen peroxide-induced endothelial hyperpermeability. Oxidative Medicine and Cellular Longevity, 2019(1), Article 1202676.
- Dudley, A. C., & Griffioen, A. W. (2023). Pathological angiogenesis: Mechanisms and therapeutic strategies. Angiogenesis, 26(3), 313–347.
- Dunaway, L. S., & Pollock, J. S. (2022). HDAC1: An environmental sensor regulating endothelial function. Cardiovascular Research, 118(8), 1885–1903.
- Duran, C. L., Borriello, L., Karagiannis, G. S., Entenberg, D., Oktay, M. H., & Condeelis, J. S. (2021). Targeting Tie2 in the tumor microenvironment: From angiogenesis to dissemination. *Cancers*, 13(22), 5730.
- English, D. M., Lee, S. N., Sabat, K. A., Baker, I. M., Pham, T. K., Collins, M. O., & Cowley, S. M. (2025). Rapid degradation of histone deacetylase 1 (HDAC1) reveals essential roles in both gene repression and active transcription. *Nucleic Acids Research*, 53(4), Article gkae1223.
- Folkman, J. (1984). Angiogenesis. Biology of endothelial cells, 412-428.
- Ganesan, P., Matsubara, K., Ohkubo, T., Tanaka, Y., Noda, K., Sugawara, T., & Hirata, T. (2010). Anti-angiogenic effect of siphonaxanthin from green alga, Codium fragile. Phytomedicine (Stuttgart): International Journal of Phytotherapy and Phytopharmacology, 17(14), 1140–1144.
- Izumi-Nagai, K., Nagai, N., Ohgami, K., Satofuka, S., Ozawa, Y., Tsubota, K., Ohno, S., Oike, Y., & Ishida, S. (2008). Inhibition of choroidal neovascularization with an anti-inflammatory carotenoid astaxanthin. *Investigative Ophthalmology & Visual Science*, 49(4), 1679–1685.
- Jeong, J. H., Ojha, U., & Lee, Y. M. (2021). Pathological angiogenesis and inflammation in tissues. Archives of Pharmacal Research, 44(1), 1–15.
- Jerka, D., Bonowicz, K., Piekarska, K., Gokyer, S., Derici, U. S., Hindy, O. A., Altunay, B. B., Yazgan, I., Steinbrink, K., Kleszczyński, K., Yilgor, P., & Gagat, M. (2024). Unraveling endothelial cell migration: Insights into fundamental forces, inflammation, biomaterial applications, and tissue regeneration strategies. ACS Applied Bio Materials, 7(4), 2054–2069.
- Kamaruddin, N. A., Fong, L. Y., Tan, J. J., Abdullah, M. N. H., Singh Cheema, M., Bin Yakop, F., & Yong, Y. K. (2020). Cytoprotective role of omentin against oxidative stress-induced vascular endothelial cells injury. *Molecules (Basel)*, 25(11), 2534.
- Kavitha, K., Kowshik, J., Kishore, T. K. K., Baba, A. B., & Nagini, S. (2013). Astaxanthin inhibits NF-κB and Wnt/β-catenin signaling pathways via inactivation of Erk/MAPK and PI3K/Akt to induce intrinsic apoptosis in a hamster model of oral cancer. Biochimica et Biophysica Acta (BBA) - General Subjects, 1830(10), 4433–4444.
- Khayyal, M. T., Teaima, M. H., Marzouk, H. M., Hazek, R. M. E., Behnam, F., & Behnam, D. (2024). Comparative pharmacokinetic study of standard astaxanthin and its micellar formulation in healthy male volunteers. *European Journal of Drug Metabolism and Pharmacokinetics*, 49(4), 467–475.
- Kikuchi, K., Dong, Z., Shinmei, Y., Murata, M., Kanda, A., Noda, K., Harada, T., & Ishida, S. (2020). Cytoprotective effect of astaxanthin in a model of normal intraocular pressure glaucoma. *Journal of Ophthalmology*, 2020(1), Article 9539681.
- Kohandel, Z., Farkhondeh, T., Aschner, M., Pourbagher-Shahri, A. M., & Samarghandian, S. (2022). Anti-inflammatory action of astaxanthin and its use in the treatment of various diseases. *Biomedicine & Pharmacotherapy*, 145, Article 112179.
- Kowshik, J., Baba, A. B., Giri, H., Reddy, G. D., Dixit, M., & Nagini, S. (2014). Astaxanthin inhibits JAK/STAT-3 signaling to abrogate cell proliferation, invasion and angiogenesis in a hamster model of oral cancer. *PLoS One*, 9(10), Article e109114.
- Krestinina, O., Baburina, Y., Krestinin, R., Odinokova, I., Fadeeva, I., & Sotnikova, L. (2020). Astaxanthin prevents mitochondrial impairment induced by isoproterenol in isolated rat heart mitochondria. *Antioxidants*, 9(3), 262.
- Küçüködük, A., Helvacioglu, F., Haberal, N., Dagdeviren, A., Bacanli, D., Yilmaz, G., & Akkoyun, I. (2019). Antiproliferative and anti-apoptotic effect of astaxanthin in an oxygen-induced retinopathy mouse model. *Canadian Journal of Ophthalmology*, 54 (1), 65–74.
- Kuehu, D. L., Fu, Y., Nasu, M., Yang, H., Khadka, V. S., & Deng, Y. (2024). Use of microalgae-derived astaxanthin to improve cytoprotective capacity in the ileum of heat-induced oxidative stressed broilers. *Animals*, 14(13), 1932.
- Kumar, S., Kumar, R., Diksha, Kumari, A., & Panwar, A. (2022). Astaxanthin: A super antioxidant from microalgae and its therapeutic potential. *Journal of Basic Microbiology*, 62(9), 1064–1082.
- Lai, T. T., Yang, C. M., & Yang, C. H. (2020). Astaxanthin protects retinal photoreceptor cells against high glucose-induced oxidative stress by induction of antioxidant enzymes via the PI3K/Akt/Nrf2 pathway. Antioxidants, 9(8), 729.
- Lee, S., Son, S. K., Cho, E., Yoo, S., Jang, E. A., & Kwak, S. H. (2024). Protective role of astaxanthin in regulating lipopolysaccharide-induced inflammation and apoptosis in human neutrophils. *Current Issues in Molecular Biology*, 46(8), 8567–8575.
- Li, J., Wang, F., Xia, Y., Dai, W., Chen, K., Li, S., Liu, T., Zheng, Y., Wang, J., Lu, W., Zhou, Y., Yin, Q., Lu, J., Zhou, Y., & Guo, C. (2015). Astaxanthin pretreatment

- attenuates hepatic ischemia reperfusion-induced apoptosis and autophagy via the ROS/MAPK pathway in mice. *Marine Drugs*, 13(6), 3368–3387.
- Liu, Z. L., Chen, H. H., Zheng, L. L., Sun, L. P., & Shi, L. (2023). Angiogenic signaling pathways and anti-angiogenic therapy for cancer. Signal Transduction and Targeted Therapy, 8(1), 198.
- Liu, Z., Li, Y., Bao, J., Li, S., Wen, Y., Zhang, P., ... Jie, Y. (2025). Astaxanthin ameliorates benzalkonium chloride-induced dry eye disease through suppressing inflammation and oxidative stress via Keap1-Nrf2/HO-1 signaling pathways. *Animal Models and Experimental Medicine*. https://onlinelibrary.wiley.com/doi/10.1002/ame2.70000.
- Liu, H., Zhang, X., Xiao, J., Song, M., Cao, Y., Xiao, H., & Liu, X. (2020). Astaxanthin attenuates d-galactose-induced brain aging in rats by ameliorating oxidative stress, mitochondrial dysfunction, and regulating metabolic markers. Food & Function, 11 (5), 4103–4113.
- Lopes-Coelho, F., Martins, F., Pereira, S. A., & Serpa, J. (2021). Anti-angiogenic therapy: Current challenges and future perspectives. *International Journal of Molecular Sciences*, 22(7), 3765.
- Manuelli, V., Pecorari, C., Filomeni, G., & Zito, E. (2022). Regulation of redox signaling in HIF-1-dependent tumor angiogenesis. FEBS Journal, 289(18), 5413–5425.
- Masoudi, A., Jorjani, M., Alizadeh, M., Mirzamohammadi, S., & Mohammadi, M. (2021). Anti-inflammatory and antioxidant effects of astaxanthin following spinal cord injury in a rat animal model. Brain Research Bulletin, 177, 324–331.
- Ng, C. T., Fong, L. Y., Tan, J. J., Rajab, N. F., Abas, F., Shaari, K., Chan, K. M., Juliana, F., & Yong, Y. K. (2018). Water extract of Clinacanthus nutans leaves exhibits in vitro, ex vivo and in vivo anti-angiogenic activities in endothelial cell via suppression of cell proliferation. BMC Complementary and Alternative Medicine, 18, 1–12.
- Nishida, Y., Berg, P. C., Shakersain, B., Hecht, K., Takikawa, A., Tao, R., Kakuta, Y., Uragami, C., Hashimoto, H., Misawa, N., & Maoka, T. (2023). Astaxanthin: Past, present, and future. *Marine Drugs*, 21(10), 514.
- Norton, K. A., & Popel, A. S. (2016). Effects of endothelial cell proliferation and migration rates in a computational model of sprouting angiogenesis. *Scientific Reports*, 6(1), Article 36992.
- Peng, Z., Pang, H., Wu, H., Peng, X., Tan, Q., Lin, S., & Wei, B. (2022). CCL2 promotes proliferation, migration and angiogenesis through the MAPK/ERK1/2/MMP9, PI3K/ AKT, Wnt/β-catenin signaling pathways in HUVECs. Experimental and Therapeutic Medicine, 25(2), 77.
- Penislusshiyan, S., Chitra, L., Ancy, I., Kumaradhas, P., & Palvannan, T. (2020). Novel antioxidant astaxanthin-s-allyl cysteine biconjugate diminished oxidative stress and mitochondrial dysfunction to triumph diabetes in rat model. *Life Sciences*, 245, Article 117367.
- Ren, L., Yang, Y., Li, W., Zheng, X., Liu, J., Li, S., Yang, H., Zhang, Y., Ge, B., Zhang, S., Fu, W., Dong, D., Du, G., & Wang, J. (2022). CDK1 serves as a therapeutic target of adrenocortical carcinoma via regulating epithelial-mesenchymal transition, G2/M phase transition, and PANoptosis. *Journal of Translational Medicine*, 20(1), 444.
- Serrano, I., Alhinho, B., Cunha, E., Tavares, L., Trindade, A., & Oliveira, M. (2023). Bacteriostatic and antibiofilm efficacy of a Nisin Z solution against co-cultures of Staphylococcus aureus and Pseudomonas aeruginosa from diabetic foot infections. *Life*, 13(2), 504.

- Shah, A. A., Kamal, M. A., & Akhtar, S. (2021). Tumor angiogenesis and VEGFR-2: Mechanism, pathways and current biological therapeutic interventions. *Current Drug Metabolism*, 22(1), 50–59.
- Sowmya, P. R. R., Arathi, B. P., Vijay, K., Baskaran, V., & Lakshminarayana, R. (2017). Astaxanthin from shrimp efficiently modulates oxidative stress and allied cell death progression in MCF-7 cells treated synergistically with β-carotene and lutein from greens. Food and Chemical Toxicology: An International Journal Published for the British Industrial Biological Research Association, 106(Pt A), 58–69.
- Speranza, L., Pesce, M., Patruno, A., Franceschelli, S., de Lutiis, M. A., Grilli, A., & Felaco, M. (2012). Astaxanthin treatment reduced oxidative induced proinflammatory cytokines secretion in U937: SHP-1 as a novel biological target. *Marine Drugs*, 10(4), 890–899.
- Sugawara, T., Matsubara, K., Akagi, R., Mori, M., & Hirata, T. (2006). Antiangiogenic activity of brown algae fucoxanthin and its deacetylated product, fucoxanthinol. *Journal of Agricultural and Food Chemistry*, 54(26), 9805–9810.
- Taïeb, J., Aranda, E., Raouf, S., Dunn, H., & Arnold, D. (2021). Clinical and regulatory considerations for the use of bevacizumab biosimilars in metastatic colorectal cancer. Clinical Colorectal Cancer, 20(1), 42–51.
- Trimm, E., & Red-Horse, K. (2023). Vascular endothelial cell development and diversity. *Nature Reviews Cardiology*, 20(3), 197–210.
- Valko, M., Rhodes, C. J. B., Moncol, J., Izakovic, M. M., & Mazur, M. (2006). Free radicals, metals and antioxidants in oxidative stress-induced cancer. *Chemico-Biological Interactions*, 160(1), 1–40.
- Wu, Y., Bashir, M. A., Shao, C., Wang, H., Zhu, J., & Huang, Q. (2024). Astaxanthin targets IL-6 and alleviates the LPS-induced adverse inflammatory response of macrophages. Food & Function, 15(8), 4207–4222.
- Xi, X., Wang, J., Qin, Y., You, Y., Huang, W., & Zhan, J. (2022). The biphasic effect of flavonoids on oxidative stress and cell proliferation in breast cancer cells. *Antioxidants*, 11(4), 622.
- Xie, D., Ju, D., Speyer, C., Gorski, D., & Kosir, M. A. (2016). Strategic endothelial cell tube formation assay: Comparing extracellular matrix and growth factor reduced extracellular matrix. *Journal of Visualized Experiments: JoVE, 2016*(114), Article 54074
- Yang, X., Guo, A. L., Pang, Y. P., Cheng, X. J., Xu, T., Li, X. R., Liu, J., Zhang, Y. Y., & Liu, Y. (2019). Astaxanthin attenuates environmental tobacco smoke-induced cognitive deficits: A critical role of p38 MAPK. Marine Drugs, 17(1), 24.
- Zhang, R., Li, H., Zhang, S., Zhang, Y., Wang, N., Zhou, H., He, H., Hu, G., Zhang, T. C., & Ma, W. (2018). RXRa provokes tumor suppression through p53/p21/p16 and PI3K-AKT signaling pathways during stem cell differentiation and in cancer cells. *Cell Death & Disease*, 9(5), 532.
- Zhu, X., Qiu, C., Wang, Y., Jiang, Y., Chen, Y., Fan, L., Ren, R., Wang, Y., Chen, Y., Feng, Y., Zhou, X., Zhu, Y., Ge, Z., Lai, D., Qin, L., Simons, M., & Yu, L. (2022). FGFR1 SUMOylation coordinates endothelial angiogenic signaling in angiogenesis. Proceedings of the National Academy of Sciences, 119(26), Article e2202631119.
- Zhu, L., Wu, H., Ma, Z., Dong, D., Yang, Z., & Tian, J. (2022). Astaxanthin ameliorates lipopolysaccharide-induced acute lung injury via inhibition of inflammatory reactions and modulation of the SOCS3/JAK2/STAT3 signaling pathways in mice. Food & Function. 13(22), 11638–11651.